Food Chemistry 444 (2024) 138684

Contents lists available at ScienceDirect

Food Chemistry

journal homepage: www.elsevier.com/locate/foodchem

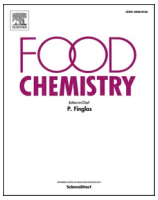

Traceability and authentication in agri-food production: A multivariate approach to the characterization of the Italian food excellence elephant garlic (*Allium ampeloprasum* L.), a vasoactive nutraceutical

Gabriele Carullo [a,b,1,*], Francesca Borghini [c,1], Fabio Fusi [a], Simona Saponara [d], Anna Fontana [a], Luca Pozzetti [a], Riccardo Fedeli [b,d], Alice Panti [d], Beatrice Gorelli [d], Giovanna Aquino [e,f], Manuela Giovanna Basilicata [e], Giacomo Pepe [e,g], Pietro Campiglia [e], Stefano Biagiotti [h], Sandra Gemma [a,b], Stefania Butini [a,b], Silvia Pianezze [i], Stefano Loppi [b,d], Alessandro Cavaglioni [c], Matteo Perini [i,2], Giuseppe Campiani [a,b,j,2,*]

[a] *Department of Biotechnologies, Chemistry and Pharmacy, University of Siena, 53100 Siena, Italy*
[b] *BioAgryLab, University of Siena, 53100 Siena, Italy*
[c] *ISVEA Srl, Istituto per lo Sviluppo Viticolo Enologico e Agroindustriale, 53036 Poggibonsi(SI), Italy*
[d] *Department of Life Sciences, University of Siena, 53100 Siena, Italy*
[e] *Department of Pharmacy, University of Salerno, 84084 Fisciano, SA, Italy*
[f] *PhD Program in Drug Discovery and Development, University of Salerno, Fisciano, SA, Italy*
[g] *NBFC, National Biodiversity Future Center, Palermo 90133, Italy*
[h] *Telematic University Pegaso, Piazza Trieste e Trento, 48 -80132 Napoli, Italy*
[i] *Experimental and Technological Services Department, Fondazione Edmund Mach, 38098 San Michele all'Adige (TN), Italy*
[j] *Bioinformatics Research Center, School of Pharmacy and Pharmaceutical Sciences, Isfahan University of Medical Sciences, Isfahan 81746-7346, Iran*

ARTICLE INFO

Keywords:
Agri-food authentication
Elephant garlic
Multivariate approach
Stable isotope ratio analysis

ABSTRACT

A research platform for food authentication was set up by combining stable isotope ratio analysis, metabolomics by gas and liquid mass-spectrometry and NMR investigations, chemometric analyses for food excellences. This multi-analytical approach was tested on samples of elephant garlic (*Allium ampeloprasum* L.), a species belonging to the same genus of common garlic (*Allium ampeloprasum* L.), mainly produced in southern Tuscany-(*Allium ampeloprasum*). The isotopic composition allowed the product to be geographically characterized. Flavonoids,

Abbreviations: ^{1}H NMR, Nuclear Magnetic Resonance; AFP, allium flavour precursors; ARA, free radical scavenging activity; CBS, Caribou Hoof Standard; CPP, coronary perfusion pressure; CSIA, Compound specific - Stable Isotope Ratio Analysis; DAD, diode array detector; DVB-CAR-PDMS, divinylbenzene-carboxy-poly-dimethylsiloxane; ECG, electrocardiogram; ESI, electrospray ionization; GSH, glutathione; HR, frequency; HS-SPME, headspace solid-phase microextraction; IRMS, isotope ratio mass spectrometer; KHS, Kudu Horn Standard; LC-HRMS, liquid chromatography-high resolution mass spectrometry; L-NAME, Nω-nitro-L-arginine methyl ester; LVP, left ventricle pressure; NCE, normalized collision energy; NO, nitric oxide; ODQ, 1*H*-[1,2,4] oxadiazole [4,3-a] quinoxalin-1-one; PCA, Principal Component Analysis; PDO, protected designation of origin; PGI, protected geographical indication; PKG, protein kinase G; PQ, atrioventricular conduction time; QRS, intraventricular conduction time; QT, overall action potential duration; RG, common garlic; RR, cycle length; SIR, Stable Isotope Ratio; SPME-GC/MS, gas chromatographic/mass spectrometric analysis; TA, elephant garlic cultivated in Tuscany; TEA, tetraethylammonium; TPC, total phenolic content; TSG, traditional specialties guaranteed; UHPLC-HRMS/MS, ultra-high performance liquid chromatography coupled to diode array detection and electrospray ionization high-resolution mass spectrometry; VA, elephant garlic sample cultivated in a northern Italian area; V-CDT, Vienna-Canyon Diablo Troilite; V-PDB, Vienna-Pee Dee Belemnite; V-SMOW, Vienna-Standard Mean Ocean Water.

* Corresponding authors at: Department of Biotechnologies, Chemistry and Pharmacy, University of Siena, 53100 Siena, Italy (G. Campiani).
E-mail addresses: gabriele.carullo@unisi.it (G. Carullo), f.borghini@isvea.it (F. Borghini), fabio.fusi@unisi.it (F. Fusi), simona.saponara@unisi.it (S. Saponara), a.fontana5@student.unisi.it (A. Fontana), luca.pozzetti@student.unisi.it (L. Pozzetti), riccardo.fedeli@student.unisi.it (R. Fedeli), alice.panti1@student.unisi.it (A. Panti), beatrice.gorelli@unisi.it (B. Gorelli), gaquino@unisa.it (G. Aquino), mbasilicata@unisa.it (M.G. Basilicata), gipepe@unisa.it (G. Pepe), pcampiglia@unisa.it (P. Campiglia), stefano.biagiotti@unipegaso.it (S. Biagiotti), gemma@unisi.it (S. Gemma), butini3@unisi.it (S. Butini), silvia.pianezze@fmach.it (S. Pianezze), stefano.loppi@unisi.it (S. Loppi), a.cavaglioni@isvea.it (A. Cavaglioni), matteo.perini@fmach.it (M. Perini), giuseppe.campiani@unisi.it (G. Campiani).
[1] Co-first authors.
[2] Co-last authors.

https://doi.org/10.1016/j.foodchem.2024.138684
Received 13 October 2023; Received in revised form 1 February 2024; Accepted 4 February 2024
Available online 8 February 2024

Glutathione
Cardiovascular activity

like (+)-catechin, cinnamic acids, quercetin glycosides were identified. The samples showed also a significant amount of dipeptides, sulphur-containing metabolites and glutathione, the latter of which could be considered a molecular marker of the analyzed elephant garlic. For nutraceutical profiling to reach quality labels, extracts were investigated in specific biological assays, displaying interesting vasorelaxant properties in rat aorta by mediating nitric oxide release from the endothelium and exhibited positive inotropic and negative chronotropic effects in rat perfused heart.

1. Introduction

Worldwide the agriculture industry is under pressure due to the increasing world population and demand for safe, and high-quality agri-food products. In the globalized agri-food system, growing segments of consumers require a trustworthy certification on the food origin, safety, and quality (Çakmakçı & Çakmakçı, 2023). At the same time, producers need to be protected by national or supranational organisms to reduce the impact of product loss or theft, adulteration, illegal sale and illegal labelling. An integrated traceability and authentication approach has become a critical component of modern food science(Gussow & Mariët, 2022, Liu et al., 2023). Food traceability identifies the capability to retrieve information about the origin and history of a food product through a supply chain. This approach allows providing evidence of a specific production chain, helping to track food in supply chains from farms to retail. Traceability criteria (food provenance, authentication and curation) have been recently pointed out (Molyneux, 2017) and a traceability system is intended to protect the identity of the regional/indigenous foods as outlined by the European Union-introduced legislation; in fact, as reported in the Council Regulation, EEC No 2081/92, there are specific names for agricultural products, foods and beverages whose quality or reputation are assessed, such as the protected designation of origin (PDO), protected geographical indication (PGI) and traditional specialties guaranteed (TSG) (Danezis et al., 2016). These definitions help producers obtain premium prices for certified products and minimize the unfair and misleading competition from fraudulent products (1151/2012 EU Regulation) (Bosona & Gebresenbet, 2013). Over the years, different strategies have been proposed for agri-food authentication, including innovative molecular approaches, molecular markers-based methods and biological investigation (Fanelli et al., 2021). Among the strategies, computational tools, principal component analyses, and spectroscopic methods, or even a variety of combinations of these techniques, have been used to "trace" foods (Olsen and Borit, 2013). During the last decade, Italy has emerged as one of the main countries involved in academic traceability studies, due to the high presence of PDO, PGI and TSG food excellences. Although these latter are quality labels, with worldwide economic impact, these categories of food are subjected to adulteration and attraction to fraudsters (Pasqualone et al., 2013; Fanelli et al., 2021). Garlic (*Allium sativum L.*) is a product with peculiar characteristics linked to its geographical origin, so that some Italian products such as Voghera garlic and Polesine white garlic are protected by the PDO (Pianezze et al., 2019). Among the different types of garlic cultivated in Italy, one of them, namely the elephant garlic (*Allium ampeloprasum* L.-Aglione) is mainly produced in southern Tuscany-Valdichiana, a traditional cultivation area (Tuscany-Valdichiana *Allium ampeloprasum* L., **TA**). Actually, **TA** has no PDO designation and it has been proposed as a substitute for garlic since its flavour is very similar to that of common garlic but with a milder impact on human breath and better digestibility (Ceccanti et al., 2021, Loppi et al., 2021). **TA** is included in the list of Traditional Agri-food Products of the Tuscany Region (Executive Decree Tuscany Region, n.1569 of April 4th, 2016) and is cited in the list of Traditional Agri-food Products of Italy (G.U. n.143 of June 21st, 2016) (Ceccanti et al., 2021), and nowadays our research platform is moving towards the assessment of quality, reputation, traceability and authentication. Elephant garlic is genetically closer to white and red garlic than to leek and presents higher fructose content and a significant amount of soluble proteins and flavonoids (Loppi et al., 2021). Moreover, a low content of fibers, which culminates in the higher digestibility of these bulbs, has been recently reported (Ceccanti et al., 2021). Several studies reported the bioactivity of (red) garlic and its extracts, pointing out their vasoactive properties (García-Villalón et al., 2016; Takashima et al., 2017) while elephant garlic has been poorly investigated. The present work is a proof of concept aimed at applying a multi-analytical approach to define the geographical authentication of **TA** and qualify its nutraceutical profile. *Allium ampeloprasum* L. is a typical food excellence from a restricted area in Tuscany where the small number of farmers cooperate within a **TA** consortium. Sampling for the present study covers bulbs cultivated in this area (Valdichiana) from ten different farmers (**TA1-TA10**) (**Fig. S1**), from soils at different altitudes. All the samples were investigated using stable isotope ratio (SIR) analysis of the major bioelements (δ^2H, δ^{13}C, δ^{15}N, δ^{18}O, δ^{34}S) to track the composition. Moreover, an elephant garlic sample cultivated in a northern Italian area (**VA**), i.e. outside the traditional cultivation area, was added to the investigated panel (**Fig. S1**). Selected **TA** samples (**TA1-TA4**) were then evaluated using solid-phase microextraction and gas chromatographic/mass spectrometric analysis (SPME-GC/MS) and compared with their alcoholic extracts (**TA1e-TA4e**). Total phenolic content (TPC) of **TAes** was determined and chemical composition of both selected **TA** samples and their extracts were further analyzed using a) liquid chromatography-high resolution mass spectrometry (LC-HRMS); b) ultra-high performance liquid chromatography coupled to diode array detection and electrospray ionization high-resolution mass spectrometry (UHPLC-HRMS/MS); and c) Nuclear Magnetic Resonance (^{1}H NMR). Glutathione was identified as a potential biomarker of **TA** grown in Tuscany. Finally, for determining the nutraceutical potential of this food excellence, **TAes** were subjected to biological assays using rat aorta rings (with or without endothelium) to assess the vasoactivity profile and one of the **TAes** was further tested in the *ex vivo* model of rat perfused heart.

2. Materials and methods

2.1. Raw samples

Elephant garlic bulbs (**TA,** 20 bulbs from ten farms for sample selection) were harvested in July 2022 from ten different local producers in the Valdichiana area as specified in the Supplementary Material. **VA** bulbs (20 bulbs from one farmer for sampling) were collected in the province of Verona while **RG** bulbs (20 samples) were purchased from one Valdichiana farmer. In each group (**TA1-10**, **VA** and **RG**) bulbs have been cultivated in the same climatic and edaphic conditions. This excludes the contribution of pedo-climatic conditions. From 20 bulbs of each provider, 20 cloves of each **TA**, 20 **VA** cloves and 20 **RG** cloves, uniform in diameter, were randomly selected, peeled, and manually triturated to obtain 12 different bulky samples. Triturated samples (**TA1-10**, **VA** and **RG**) were freeze-dried using freeze-dryer Lio SP (5Pascal, Milan, Italy) equipped with a Edwards RV3 oil vacuum pump (operating conditions: T= − 50 °C, P = 0.2 mbar).

2.2. Stable isotope ratio (SIR) analysis

Freeze-dried elephant garlic samples were analyzed by measuring the ^{13}C/^{12}C, ^{15}N/^{14}N and ^{34}S/^{32}S ratios by using an isotope ratio mass spectrometer (IsoPrime, Isoprime Limited, Germany) after total

combustion in an elemental analyser (VARIO CUBE, Isoprime Limited, Germany). The $^{2}H/^{1}H$ and $^{18}O/^{16}O$ ratios were measured using an isotope ratio mass spectrometer (IRMS) (Finnigan DELTA XP, Thermo Scientific) coupled with a pyroliser (Finningan DELTA TC/EA, high-temperature conversion elemental analyser, Thermo Scientific). To analyse the samples, the amount introduced in the instruments was 0.5 mg for $\delta^{13}C$, $\delta^{15}N$ and $\delta^{34}S$, and 0.2 mg for $\delta^{2}H$ and $\delta^{18}O$ respectively. The values (see Table 1) are denoted in delta in relation to the international V-PDB (Vienna-Pee Dee Belemnite) for $\delta^{13}C$, V-SMOW (Vienna-Standard Mean Ocean Water) for $\delta^{2}H$ and $\delta^{18}O$, Air for $\delta^{15}N$ and V-CDT (Vienna-Canyon Diablo Troilite) for $\delta^{34}S$ according to the following general equation:

$$\delta_{ref}\left({}^{i}E/{}^{j}E, sample\right) = \left[\frac{R({}^{i}E/{}^{j}E, sample)}{R({}^{i}E/{}^{j}E, ref)}\right] - 1 \quad (1)$$

where *ref* is the international measurement standard, *sample* is the analysed sample and ${}^{i}E/{}^{j}E$ is the isotope ratio between heavier and lighter isotope. The delta values are multiplied by 1000 and expressed commonly in units "per mil" (‰) or, according to the International System of Units (SI), in unit 'milliurey' (mUr). The isotopic values were calculated against two standards through the creation of a linear equation. The standards that have been used in the isotopic analyses were international reference materials or in − house working standards that have been calibrated against them.

In particular, the international standards that have been used are: for $^{13}C/^{12}C$, fuel oil NBS − 22 ($\delta^{13}C = -30.03 \pm 0.05$ ‰), sucrose IAEA − CH − 6 ($\delta^{13}C = -10.45 \pm 0.04$ ‰) (IAEA − International Atomic Energy Agency, Vienna, Austria), and L − glutamic acid USGS 40 ($\delta^{13}C = -26.39 \pm 0.04$ ‰) (U.S. Geological Survey, Reston, VA, USA); for $^{15}N/^{14}N$, L − glutamic acid USGS 40 ($\delta^{15}N = -4.52 \pm 0.06$ ‰) (U.S. Geological Survey, Reston, VA, USA), ammonium sulfate salts IAEA − N − 1 ($\delta^{15}N = +0.43 \pm 0.07$ ‰) and IAEA − N − 2 ($\delta^{15}N = +20.41 \pm 0.12$ ‰) and potassium nitrate IAEA − NO3 ($\delta^{15}N = +4.7 \pm 0.2$ ‰); for $^{34}S/^{32}S$, USGS 42 ($\delta^{34}S = +7.84 \pm 0.25$ ‰), USGS 43 ($\delta^{34}S = +10.46 \pm 0.22$ ‰), barium sulphate IAEA − SO − 5 ($\delta^{34}S = +0.5 \pm 0.2$ ‰) and NBS 127 ($\delta^{34}S = +20.3 \pm 0.4$ ‰); for $^{2}H/^{1}H$ fuel oil NBS − 22 $\delta^{2}H = -119.6 \pm 0.6$ ‰) and keratins CBS (Caribou Hoof Standard $\delta^{2}H = -157 \pm 2$ ‰) and KHS (Kudu Horn Standard $\delta^{2}H = -35 \pm 1$ ‰) from U.S. Geological Survey; for $^{18}O/^{16}O$ benzoic acid IAEA 601 ($\delta^{18}O = +23.14 \pm 0.19$ ‰) and benzoic acid IAEA 602 ($\delta^{18}O = +71.28 \pm 0.36$ ‰) from IAEA.

Each reference material was measured in duplicate at the start and end of each daily group of analyses of samples (each sample was also analyzed in duplicate). A control material was also included in the analyses of each group of samples, to check the efficiency of the measure. The maximum standard deviations of repeatability accepted were 0.3 ‰ for $\delta^{13}C$ and $\delta^{15}N$, of 0.4 ‰ for $\delta^{34}S$, 0.5 ‰ for $\delta^{18}O$ and of 3 ‰ for $\delta^{2}H$.

Table 1
Values and relative means and standard deviations of the different isotopic ratios measured in TA and VA samples. T-test for single means was applied. Different letters (a or b) indicate significant differences between the experimental groups ($p < 0.05$).

	$^{2}H/^{1}H$ ($\delta^{2}H$) (‰ vs V-SMOW)	$^{13}C/^{12}C$ ($\delta^{13}C$) (‰ vs V-PDB)	$^{15}N/^{14}N$ ($\delta^{15}N$) (‰ vs AIR)	$^{18}O/^{16}O$ ($\delta^{18}O$) (‰ vs V-SMOW)	$^{34}S/^{32}S$ ($\delta^{34}S$) (‰ vs V-CDT)
TA1	−46 ± 1.2	−26.0 ± 0.1	5.8 ± 0.2	36.9 ± 0.2	2.2 ± 0.4
TA2	−44 ± 0	−26.1 ± 0.2	2.2 ± 0.2	35.4 ± 0.6	7.1 ± 0.1
TA3	−46 ± 1	−27.4 ± 0.1	2.2 ± 0.1	36.3 ± 0.5	6.1 ± 0.2
TA4	−49 ± 0	−27.3 ± 0.1	1.2 ± 0.2	36.0 ± 0.2	2.7 ± 0.2
TA5	−59 ± 1	−28.2 ± 0.1	4.5 ± 0.2	36.4 ± 0.2	5.2 ± 0.2
TA6	−62 ± 2	−27.0 ± 0.1	4.0 ± 0.1	35.3 ± 0.5	2.3 ± 0.3
TA7	−52 ± 1	−25.4 ± 0.1	6.3 ± 0.2	31.8 ± 0.1	2.2 ± 0.2
TA8	−63 ± 1	−27.9 ± 0.1	5.9 ± 0.2	28.0 ± 0.4	−3.4 ± 0.1
TA9	−61 ± 3	−27.8 ± 0.2	5.6 ± 0.1	28.4 ± 0.5	10.6 ± 0.1
TA10	−41 ± 2	−28.9 ± 0.3	4.4 ± 0.2	29.3 ± 0.2	5.2 ± 0.3
Mean	−52[a]	−27.2[a]	4.2[a]	33.4[a]	4.0
SD	9	1.1	1.8	3.7	3.8
VA	−34 ± 2[b]	−27.4 ± 0.2[a]	−1.5 ± 0.1[b]	31.7 ± 0.2[a]	ND

ND: Not Determined.

2.3. Extracts and extraction procedure

Selected **TA** bulbs, namely **TA1**, **TA2**, **TA3** and **TA4** (500 g) were manually peeled, triturated and then macerated with methanol (HPLC grade, purity > 95 %, 1000 mL). After 72 h the liquid was filtered, and the solvent was removed to obtain: **TA1e-TA4e.** Samples were then freeze-dried and stored at −20 °C. The extracts obtained using maceration with methanol were quantified: **TA1e**, 50.1 g (yield 10.02 %), **TA2e**, 38.1 g (yield 7.62 %), **TA3e**, 29.6 g (yield 5.92 %) and **TA4e**, 41.5 g (yield 8.21 %).

2.4. SPME-GC/MS analysis of volatile compounds

Volatile compounds were extracted from freeze-dried **TA1-4** and **TA1e-TA4e** using headspace solid-phase microextraction (HS-SPME) and analyzed by GC/MS. SPME fibre holder and 50/30 nm divinylbenzene-carboxy-polydimethylsiloxane (DVB-CAR-PDMS) fibres were purchased from Supelco (Bellefonte, PA, USA). GC samples were diluted fourfold, and 4 mL of each solution was placed in a 10-mL glass vial. A volume of 50 μL of internal standard solution and 1 g of ammonium sulphate were added. The vial was sealed with a Teflon-faced septum cap, and the sample was pre-conditioned at 40 °C for 15 min. Microextraction lasted for 40 min at 40 °C with stirring (800 rpm). For desorption, the fibre was inserted into the GC/MS injector port at 248 °C for 5 min (3 min in splitless mode). Identification and quantification of volatile compounds were performed using a Thermo Scientific (Waltham, MA, USA) Trace 1300 gas chromatograph coupled with a single quadrupole mass spectrometer (ISQ 7000, Thermo Scientific, Waltham, MA, USA). The column used was an Rtx-WAX (60 m × 0.25 mm i.d., 0.25 μm fi lm thickness; Restek, Bellefonte, PA, USA). The initial oven temperature was 40 °C, then increased at 2 °C/min to 240 °C, and then kept at 240 °C for 10 min. Injector, transfer line and ion trap temperatures were 245, 180 and 120 °C, respectively. Identification was performed by comparing retention times and mass spectra with those of pure standards, when in house available, and with mass spectra from NIST05 library (National Institute of Standards and Technology, Gaithersburg, MD, USA), as described in Supplementary Material.

2.5. HPLC-HRMS targeted analysis

The raw freeze-dried **TA1-4, VA** and **RG** and freeze-dried **TA1e-TA4e** samples were extracted with methanol solution (80:20, 1:10 wt: volume ratio) for 15 min at room temperature in an ultrasound apparatus. The extracts were centrifuged (3500 rpm for 10 min), and then the supernatants were filtered by syringe filters (0.22 μm) before the LC-HRMS analysis. **TA1-TA4** and **TA1e-TA4e** were analyzed for the content of phenolic compounds and glutathione using LC-HRMS, coupled with a diode array detector (DAD) (Ultimate 3000, Dionex, Thermo Fisher Scientific (Waltham, MA, USA)). All samples and standards were handled to minimize light exposure. The samples were filtrated to 0.45 μm and then analyzed, without any other preparation step. The liquid

chromatograph was an Accela (Accela 1250, Thermo Fisher Scientific (Waltham, MA, USA) equipped with a quaternary pump and a thermostated autosampler. A kinetex F5 column (2.1 × 100 mm 1.7 μm; Phenomenex (Torrance, CA, USA)) was used. The autosampler tray temperature was set at 10 ∘C, and the column at 40 ∘C. Gradient elution was performed with water / 0.1 % formic acid / 5 mM ammonium formate (solvent A) and methanol/0.05 % formic acid / 5 mM ammonium formate (solvent B) at a constant flow rate of 400 μL/min, and the injection volume was 3 μL. An increasing linear gradient of solvent B was used. Separation was carried out in 45 min under the following conditions: 0 min, 5 % B; 13 min, 5 % B; 22 min, 35 % B; 24 min, 35 % B; 27 min, 90 %; 32 min 90 % B and from 33 min to 45 min, 5 % B. An LTQ Orbitrap Exactive mass spectrometer (Thermo Fisher Scientific, (Waltham, MA, USA)) equipped with an electrospray ionization (ESI) source in negative mode was used to acquire mass spectra in full mass spectrometry (MS) data-dependent MS2 experiment. Further details are reported in Supplementary Material.

2.6. HPLC-HRMS untargeted analysis

The samples were analyzed by a Vanquish™ Flex UHPLC Systems (Thermo Fisher Scientific, Bremen, Germany) coupled with an Orbitrap Exploris 120 mass spectrometer (Thermo Fisher Scientific, Bremen, Germany). For untargeted analysis, a Thermo Scientific™ C18 Hypersil™ ODS column (2.1 mm*15 mm, 1.7 μm) was used. The metabolite identification was performed using a mix of accurate mass, MS^2 spectra, FISh coverage and database matching. Moreover, compounds were mapped to biological pathways using Metabolika. Further details are reported in Supplementary Material.

2.7. UHPLC-HRMS/MS quantitative analysis of dipeptides in TA1e-TA4e samples

UHPLC-HRMS/MS analysis was performed on a Thermo Ultimate RS 3000 coupled online to a Q-Exactive hybrid quadrupole Orbitrap mass spectrometer (Thermo Fisher Scientific, Bremen, Germany) equipped with a heated electrospray ionization probe (HESI II). The chromatographic separation was accomplished on an ACQUITY UPLC HSS T3 (150 × 2.1 mm × 1.8 μm) (Waters, Milan, Italy) analytical column maintained at 40 °C. The mobile phase consisted of H_2O (A) and ACN (B), both acidified with 0.1 % v/v formic acid (FA) delivered at a constant flow of 0.3 mL min^{-1}. The analysis was performed using a gradient elution method with the following conditions: 0.01–20.00 min, 5–20 % B; 20.01–30.00 min, 20–95 % B; 30.01–33.00 min, isocratic to 95 % B; 33.01–35.00 min, 5 % B; followed by five minutes for column re-equilibration. The ESI was operated both in negative and positive mode. The MS was calibrated by Thermo calmix Pierce™ calibration solutions in both polarities. Full MS (50–500 *m/z*) and data-dependent MS/MS were performed at a resolution of 35,000 and 17,500 FWHM respectively, and normalized collision energy (NCE) values of 15, 20, and 25 were used. Source parameters: Sheath gas pressure, 50 arbitrary units; auxiliary gas flow, 13 arbitrary units; spray voltage, +3.5 kV, −2.8 kV; capillary temperature, 310 °C; auxiliary gas heater temperature, 300 °C. The quantification of dipeptides content in **TA1e-TA4e** was performed using a Shimadzu Nexera UHPLC system (Tokyo, Japan) consisting of a SIL-30AC autosampler, a CBM-20A controller, a DGU-20 AR5 degasser, two LC-30AD pumps, a CTO-20AC column oven and an SPD-M20A photodiode array detector (further details in Supplementary Material).

2.8. ^1H NMR analysis

NMR analysis was conducted on a Varian 300 MHz spectrometer (Milan, Italy) by diluting 10 mg of **TA1e-TA4e** samples in 600 μL of deuterium oxide (D_2O). The resonances were assigned by analyzing ^1H NMR characteristics and by comparison with the literature and databanks.

2.9. Total polyphenols content (TPC)

TPC was determined following a method previously described (Fedeli, Celletti, et al., 2023). Freeze-dried samples (100 mg) were homogenized with 4 mL of 70 % acetone and centrifuged at 4000 rpm for 5 min. The supernatant (0.5 mL) was combined with 3 mL of dH_2O, 0.125 mL of Folin–Ciocalteau reagent, 0.750 mL of saturated Na_2CO_3, and finally 0.950 mL of dH_2O. The samples were incubated at 37 °C for 30 min, followed by centrifugation at 4000 rpm for 5 min. Their absorbance was measured at 765 nm using a UV–Vis spectrophotometer (8453, Agilent, Santa Clara, CA, USA). Quantification was performed by comparing the absorbance of the samples to a calibration curve (ranging from 5 to 20 μg mL^{-1}) with gallic acid as the standard.

2.10. Free radical scavenging activity (ARA)

ARA content was determined following a previously described method (Fedeli, Vannini, et al., 2023). Freeze-dried samples (100 mg) were homogenized with 2 mL of 80 % ethanol and centrifuged at 15,000 for 5 min. An aliquot of the supernatant (200 μL) was added to 1 mL of a 2,2-Diphenyl-1-picrylhydrazyl solution, which was prepared by dissolving 1.85 mg of DPPH in 50 mL of 80 % methanol. Following a reaction period of 1 h, the samples underwent spectrophotometric analysis (8453, Agilent, Santa Clara, CA, USA) at a wavelength of 517 nm. The results were expressed as ARA% using the formula:

$$ARA\% = [1 - (sampleAbs/controlAbs)] \times 100$$

where *control Abs* is the absorbance of the reagents only.

2.11. Animals

Animal study procedures were in strict accordance with the European Union Guidelines for the Care and the Use of Laboratory Animals (European Union Directive 2010/63/EU) and approved by the Animal Care and Ethics Committee of the University of Siena and the Italian Department of Health (7DF19.N.TBT). Male Wistar rats (260–360 g; n = 42), purchased from Charles River Italia (Calco, Italy), were maintained in an animal house facility at 25 ± 1 °C and a 12:12 h dark-light cycle, fed a standardised diet and provided drinking water *ad libitum*. Animals were anaesthetized with isoflurane (4 %)–O_2 gas mixture using Fluovac equipment (Harvard Apparatus, Holliston, Massachusetts, USA), decapitated, and exsanguinated. The thoracic aorta was immediately isolated, placed in a modified Krebs-Henseleit solution (KHS) and prepared as detailed in sections 2.12.

2.12. Aorta ring preparation

The thoracic aorta was gently cleaned of adipose and connective tissues and cut into 3–4-mm wide rings. These were mounted in organ baths between two parallel, L-shaped, stainless-steel hooks, one fixed in place and the other connected to an isometric transducer. Rings were allowed to equilibrate for 60 min in KHS (composition in mM: 118 NaCl, 4.75 KCl, 1.19 KH_2PO_4, 1.19 $MgSO_4$, 25 $NaHCO_3$, 11.5 glucose, 2.5 $CaCl_2$, gassed with a 95 % O_2-5 % CO_2 gas mixture to create a pH of 7.4) under a passive tension of 1 g (Carullo et al., 2021). During this equilibration period, the solution was changed every 15 min. Isometric tension was recorded using a digital PowerLab data acquisition system (PowerLab 8/30; ADInstruments). Ring viability was assessed by recording the response to 0.3 μM phenylephrine and 60 mM KCl. Where needed, the endothelium was removed by gently rubbing the lumen of the ring with a forceps tip. This procedure was validated by adding 10 μM acetylcholine at the plateau of phenylephrine-induced contraction: a relaxation ≥ 75 % or less than 15 % denoted the presence or absence of

functional endothelium, respectively (Ahmed et al., 2023).

2.13. Evaluation of TA1e-TA4e on phenylephrine- and high KCl-induced contractions

Aorta rings were pre-contracted pharmaco-mechanically with 0.3 μM phenylephrine (endothelium-intact or denuded) or electro-mechanically with 25–35 mM or 60 mM KCl (endothelium-denuded). (Fusi et al., 2008) Once the contraction reached a plateau, extracts were added cumulatively into the organ bath to assess their vasorelaxant activity. In some experiments, preparations were pre-incubated with 100 μM Nω-nitro-L-arginine methyl ester (L-NAME) or 1 μM 1*H*-[1,2,4] oxadiazole [4,3-*a*] quinoxalin-1-one (ODQ) for 20 min before the addition of phenylephrine, or 1 mM tetraethylammonium (TEA) for 20 min before the addition of 25 mM KCl, respectively. At the end of the concentration–response curve, 100 μM sodium nitroprusside alone (phenylephrine-induced contraction) or 1 μM nifedipine followed by sodium nitroprusside (KCl-induced contraction) were added to test the functional integrity of smooth muscle. Vasodilation was calculated as a percentage of the contraction induced by either phenylephrine or KCl (taken as 100 %).

2.14. Evaluation of TA1e on Ca^{2+} release from intracellular stores and extracellular Ca^{2+} influx triggered by phenylephrine

Rings were pre-incubated with 1 mg mL^{-1} **TA1e**, first for 30 min in normal KHS, and then for 5 min in a Ca^{2+}-free KHS containing 1 mM EGTA. The subsequent addition of 10 μM phenylephrine (this maximal concentration was required to obtain a measurable contraction in the absence of extracellular Ca^{2+}) evoked a contraction representing the release of Ca^{2+} from the sarcoplasmic reticulum. The following addition of 3.5 mM Ca^{2+} caused a further contraction due to the influx of extracellular Ca^{2+}.(Fusi et al., 2015; Pozzetti et al., 2022) As the concentration of phenylephrine was higher than that used in the viability tests (see above), responses were measured as a percentage of the contraction induced by 60 mM KCl in KHS.

2.15. Effects of TA1e on Langendorff perfused rat heart

Spontaneously beating heart, mounted on a constant flow Langendorff apparatus for retrograde perfusion via the aorta, was allowed to equilibrate for at least 20 min before **TA1e** exposure. Cardiac contractile performance was assessed by measuring the left ventricle pressure (LVP), placing a deionized water-filled latex balloon into the left ventricle through the mitral valve and connecting it to a pressure transducer (BLPR, WPI, Berlin, Germany). Changes in coronary perfusion pressure (CPP), originating from alterations in coronary vascular resistance, were monitored using a pressure transducer (BLPR, WPI, Berlin, Germany) positioned within the inflow line (Pessina et al., 2018). A surface electrocardiogram (ECG) was recorded at a sampling rate of 1 kHz using two steel electrodes One electrode was positioned at the apex of the heart, while the other was on the left atrium. The ECG analysis included the following parameters: HR (frequency), RR (cycle length), PQ (atrioventricular conduction time), QRS (intraventricular conduction time), and QT (overall action potential duration) (Saponara et al., 2007; Fusi et al., 2017).

2.16. Statistical analysis

Analysis of the data was accomplished with GraphPad Prism version 5.04 (GraphPad Software Inc.). Data normality was checked with the Shapiro-Wilk test. Data are reported as mean ± SD; n is the number of hearts or rings analysed isolated from at least three animals. E_{max} values represent the maximum response achieved with the highest concentration tested. For the statistical significance of Student's *t* tests for unpaired samples (two-tailed) or ANOVA and Dunnett post-hoc tests a $P < 0.05$ level was considered. Means were compared using Tukey's HSD (Statgraphics Centurion 18, Stat Point Technologies, Inc., Warrenton, VA, USA). Significance was considered at $p < 0.05$. Means with different alphabetical letters in the same column of the table are considered statistically different at 95 % confidence level. Major patterns of variation in the targeted and untargeted chemical data were explored using Principal Component Analysis (PCA), with centring and standardization of the variables. PCA is a technique for reducing the complexity of a large number of variables into some uncorrelated latent variables (principal components) which represent the greatest possible share of the variance present in the data. Multivariate analysis was performed using PLS_Toolbox (Eigenvector Research, Inc., Manson, WA,USA).

3. Results and discussion

3.1. Variation of δ^2H, $\delta^{213}C$, $\delta^{18}O$, $\delta^{15}N$, $\delta^{34}S$ across different areas

SIR analysis has been used in recent decades for the authentication and traceability of different foodstuffs, such as wine, vegetables, meat and spices. The bulk SIR and compound-specific stable isotope analysis (CSIA) have been successfully applied in this field to discriminate samples coming from different origins and/or to give information about the food production chain (Liu et al., 2023). SIR analysis has been applied by some authors for characterizing garlic (*Allium sativum* L.) from different geographical areas of China (Nie et al., 2021) and other Eastern countries, (*Sen* Liu et al., 2018) of Argentina (Nie et al., 2021), of Slovenia(Opatić et al., 2017), and of Italy (Pianezze et al., 2019). The $\delta^{13}C$ values of **TA** samples range from −28.9 to −25.4 ‰ (Table 1). Similar variability ranges (from −29.9 to −24.4 ‰) were reported by Liu *et al.* for *Allium sativum* L. samples (from −28.5 to −25.6 ‰) from Argentina and Asia, by Opatić *et al.* for samples from Slovenia (Opatić et al., 2017; Liu et al., 2018) and by Pianezze *et al.* (from −27.1 to −24.6 ‰) for Italian samples (Pianezze et al., 2019). This behaviour is in line with the botanical origin of the matrix, indeed while C4 plants have $\delta^{13}C$ values between −14 and −12 ‰, C3 plants (such as garlic) range from −30 to −23 ‰. Excluding a possible intragenus effect on the isotopic composition between *Allium ampeloprasum L.* and *Allium sativum L.* which should be evaluated in a specific study, comparing the values of this study on a national scale with the values reported for other Italian regions by Pianezze *et al.*, it is possible to note how the Tuscan samples (**TA**) studied here (mean −27.2 ‰) and the sample from Veneto (**VA**) differ significantly from the Sicilian garlic (with mean values −25 ‰) ($p < 0.05$) while they tend to be more negative, although not significantly different from those of central Italy (Abruzzo and Lazio). This behaviour is mainly due to the effect of the different latitude and therefore the different climatic conditions (more extreme in the south than in the north of Italy) on the carbon isotope ratio. The temperature dependence can be explained by considering both the changes in the coefficient of CO_2 utilization at different temperature conditions and the result of the thermodynamically ordered distribution of isotopes in biological systems. The different climate influences the stomatal opening and closing of the same plant grown in different areas, inducing a concentration or depletion of the heavier isotope with effects on the $^{13}C/^{12}C$ ratio. This justifies the lower values recorded in the **TA** samples (Pianezze et al., 2019).

As reported in the literature, oxygen and hydrogen isotopic ratios depend on many variables, such as geographical origin, altitude, latitude, and proximity to the sea (Bowen et al., 2007). It is well known that hydrogen and oxygen isotopic values are strictly correlated in precipitation/meteoric water (Araguas Araguas et al., 1996) while in plant water this correlation is still valid even if it is not so close. Indeed, in a plant, water is the only source of hydrogen, while, oxygen may derive from O_2 and CO_2 (Barbour, 2007). This explains the low correlation between the two parameters recorded in the analyzed samples. Comparing the samples of **TA** with those of garlic from other Italian regions, it is noted that both δ^2H and $\delta^{18}O$ parameters are significantly

different between **TA** samples (average respectively −52 ‰ and + 33 ‰) and the Sicilian one (average −38 ‰ and + 30 %) while the values tend to overlap with those measured in samples from central Italy.

To evaluate the correlation with the isotopic signature of rainfall, in the absence of direct measurement of the δ^2H and δ^{18}O of rainwater, we used water isotope data from the k administered by Gabriel Bowen. The data available in the database http://wateriso.utah.edu are the monthly weighted average precipitation values for sites all over the world. The rainwater in the Tuscan sampling areas has an average δ^2H of −39 ‰ and an average δ^{18}O of −6.4 ‰ while in the Sicilian site sampled by Pianezze *et al.*(Pianezze et al., 2019) are equal to −31 ‰ and −5.3 ‰ respectively. This significant difference together with the difference in altitude (approximately 300 m for the Tuscan sites compared to sea level for the Sicilians) is reflected in the isotopic ratios measured on the garlic samples with different significances because the only source of hydrogen is water while oxygen also derives from O_2 and CO_2 (Barbour, 2007).

Liu *et al.* carried out a study about the discrimination between garlic samples coming from Argentina and some countries in Asia (Liu et al., 2018). Hydrogen and oxygen isotopic ratios were fundamental to discriminate between Argentinian and Asian samples. As the first ones had δ^2H values ranging between −102.5 and −85.5 ‰ and δ^{18}O values ranging between 21.1 and 25.5 ‰, while the second ones had δ^2H values ranging between −70.3 and −35.7 ‰ and δ^{18}O values ranging between 25.1 and 32.9 ‰, the two groups were distinguishable. Both δ^2H and δ^{18}O values of **TA** samples (ranging between −63 and −41 ‰ for hydrogen and between 28.0 and 36.9 ‰ for oxygen) are significantly different from the samples from Argentina, however, it is not possible to discriminate them against Asian garlic samples.

The main factor affecting δ^{15}N in cultivated plants is the fertilization process used. Synthetic fertilizers, produced from atmospheric nitrogen via the Haber process, have δ^{15}N values between −4 and + 4 ‰, while organic fertilizers are characterized by values between + 0.6 and + 36.7 ‰ (Bateman et al., 2007). δ^{15}N values of **TA** samples range from + 1.2 ‰ to + 6.3 ‰ (Table 1) therefore presenting values not dissimilar to those reported for samples of Italian garlic (between −3.0 and + 7.6 ‰) (Pianezze et al., 2019). The high isotopic variability found reflects the alternative use of various types of fertilizers as there is not yet a specification that suggests a specific one. However, the absence of negative values, found instead by Pianezze *et al.*, (Pianezze et al., 2019) seems to indicate a tendency towards non-fertilization or the use of organic fertilizers. Liu *et al.* reported a higher isotopic range for δ^{15}N (between 4.4 and 9.8 ‰) for samples from Argentina probably due to the use of non-chemical fertilizers (Liu et al., 2018). On the contrary, the range reported for Asia (between −2.4 and + 8.4 ‰) and for Slovenia (between 0.1 and 12.3 ‰) (Opatić et al., 2017) overlaps that found in the Italian garlic data. The sulphur isotopic ratio is influenced by many different factors, such as an abundance of sulphides in soil, plants' aerobic and anaerobic growth, local bedrocks,(Rubenstein & Hobson, 2004) active microbial process in the soil, fertilization procedures, and active deposition. δ^{34}S values of **TA** samples range from −3.4 ‰ to + 10.6 ‰ therefore presenting values not dissimilar to those reported for samples of Italian garlic (between −5.1 and + 12 ‰) (Pianezze et al., 2019). The results found for Slovenian samples are perfectly analogous to ours for δ^{34}S (Slovenian values between −4.0 and 7.1 ‰).

3.2. Analysis of elephant garlic and common garlic volatile metabolites via SPME-GC/MS

SPME-GC/MS analysis was used to analyze the presence of volatile compounds on freeze-dried **TA** samples and corresponding **TAes**. Row **TA** sample and **TAe** showed superimposable spectra (**Fig. S2**). As expected, the main metabolites identified by the SPME-GC/MS analysis of the **TA** samples fall into the group of volatile sulphides, such as diallyl sulphide, diallyl disulphide, allyl trisulphide, which are decomposition products of the highly unstable allicin, and allyl methyl disulphide and trisulphide. In particular, these compounds represent the main components of all the samples, accounting for more than 50 % of the total identified compounds, up to 92.24 % and 89.88 % in the case of **TA3** and **TA4**, respectively (Table 2).

Tetramethylene sulphide (17.15 %) has been identified in **TA2**, but not in the extract **TA2e** due to its volatility. Other organosulfur compounds belonging to the dithiins class, such as 3-ethenyl-1,2-dithi-4-ene, are present in **VA** and **RG**, the former, and in **TA2e**, the latter (Table 2). In summary, **TA** does not contain 1,2-dithiole and 3-ethenyl-1,2-dithi-4-ene.

3.3. Quantitation of metabolites in TA1-TA4, VA, RG and TA1e-TA4e by HPLC-HRMS analysis

To assess the chemical composition of the whole panel of samples, HPLC-HRMS targeted analysis was performed. As reported in Table 3, (+)-catechin was detected in all the samples, but in a low amount (<0.050 mg/Kg). Caffeic acid was detected in all the samples, but only **TA1e** showed an appreciable amount (3.375 mg/Kg), followed by **TA2** and **TA2e** (2.202 and 2.782 mg/Kg, respectively). Caffeic acid analogues, namely coumaric and ferulic acids, have been found in all the samples. In particular, ferulic acid is highly present in **TA4e** (11.41 mg/Kg). Quercetin glycosides have been detected in low amounts; in particular, quercetin-3-O-glucuronide was found in traces only in **TA2e**-**TA4e** (<0.050 mg/Kg). Quercetin-3-O-rutinoside has been detected especially in the **RG** sample (common garlic) while abscisic acid was found in all the samples. Glutathione (GSH) was particularly detected in **TA3**, **TA4** and their corresponding methanol extracts **TA3e**,**TA4e** (26,18–36,36 mg/Kg).

3.4. Identification and analysis of candidate metabolites and chemometric analysis (PCA)

To analyze the different metabolites present in the samples, a metabolomic analysis was performed identifying selected bioactives using computational tools. **Table S1** lists the 109 elephant garlic chemical ingredients detected and identified by metabolomic HPLC-HRMS analysis. The metabolomic profiles are summarized in **Fig. S3**. **Fig. S3A** highlights the composition of all **TA** while **Fig. S3B** reports the percentage composition of **RG**. **TA** clearly shows higher levels of sugars and sulfur-containing molecules not belonging to the super pathway of Allium flavour precursors (AFP). Regarding the AFP metabolic pathway, 18 compounds out of the 48 molecules of AFP (Li et al., 2022) were identified by HPLC-HRMS analysis in elephant garlic samples (**Table S1**). The PCA plots of sulfur-containing volatile compounds detected by GC–MS and by HPLC-HRMS are shown in Fig. 1. In both cases, the first two axes explain more than 75 % of the total variability, of which PC1 was the most significant, explaining about 54 % of the total variability in both analyses (Fig. 1**A-B**). A clear sample separation can be observed in both cases along PC1, with **TA** samples on the negative side of PC1 and **VA** on the opposite quarter, the latter more similar to the common garlic sample than to the Tuscany samples. Sixteen major volatile compounds were detected by GC–MS and **TA1-4** generally showed lower levels of sulfur-containing volatile compounds, according to literature results (Kim et al., 2017). Concerning the untargeted results, the variables (Fig. 1**C**) that more influence the sample assemblage in the metabolomic analysis are above all the different distribution of sulfur-containing molecules and the higher sugar levels in **TA** samples than in the other allium types (Li et al., 2022). Two sugars (maltotriose and galactose), the sulfur compound *N*-γ-L-glutamyl-L-methionine and the glutamyl-*S*-(1E)-1-propen-1-yl-L-cysteine, a precursor of AFP, were found to be the main metabolites along the negative side of component 1 in the PCA, being these compounds highly characterizing **TA** samples. **TA** showed higher levels of typical sulfur-containing compounds, while methionine, S-methyl-L-cysteine-S-oxide, S-allyl-L-cysteine and alliin characterize **VA** and **RG** (Fig. 1**D**). An abundance of N-γ-L-glutamyl-L-methionine, an organosulfur compound with antidiabetic, anticancer,

Table 2
Volatile compounds identified in **TA1-TA4**, **VA**, **RG** and **TA1e-TA4e**. The second column reports the NIST spectral match values in percentage.

Components	NIST match	Samples and relative %									
		TA1	TA1e	TA2	TA2e	TA3	TA3e	TA4	TA4e	VA	RG
Trimethylene	85	1.05	1.54	0.91	3.68	0.99	2.80	1.08	3.92	3.74	1.86
Acetaldehyde	93	0.17	0.20	0.11	0.14	0.19	0.27	0.23	0.28	0.34	0.04
Allyl mercaptan	87	1.87	2.95	1.19	3.83	1.84	9.39	1.93	5.71	17.48	2.03
Diallyl sulphide	88	2.02	1.60	4.35	5.80	1.77	4.61	2.05	2.47	3.08	2.16
Allyl methyl disulphide	84	25.71	4.12	7.07	1.34	35.92	4.38	37.06	5.81	32.35	15.86
Tetramethylene sulphide	88	n.d	n.d.	17.15	n.d.	n.d.	n.d.	n.d.	n.d.	n.d.	n.d.
Dimethyl trisulphide	91	0.91	5.48	n.d.	n.d.	1.05	3.94	2.20	4.16	2.82	3.70
trans-2-ethyl-3-methylthiophane	83	n.d.	0.56	n.d.	0.24	n.d.	0.32	n.d.	0.04	0.20	n.d.
1-allyl-2-isopropyldisulphane	86	12.49	0.74	3.60	0.39	4.88	0.38	2.20	0.53	0.29	0.36
Diallyl disulphide	93	40.34	33.79	63.19	42.72	40.59	37.45	37.85	37.90	4.47	46.46
1,2-Dithiole	85	0.88	2.49	0.35	2.09	0.65	2.06	0.77	4.24	11.07	6.65
Allyl methyl trisulphide	89	5.83	21.79	0.39	7.23	7.38	21.29	11.55	20.80	10.84	9.20
Allyl propyl trisulphide	88	4.01	6.21	0.09	5.86	1.12	1.96	0.19	1.90	1.08	0.44
3-ethenyl-1,2-dithi-4-ene	81	2.81	4.00	0.72	7.77	1.66	3.53	1.23	3.59	9.18	4.75
Allyl trisulphide	84	1.60	4.14	0.65	6.56	1.70	5.17	1.22	4.12	n.d.	5.12
Methyl palmitate	92	n.d.	5.19	n.d.	4.95	n.d.	0.97	n.d.	1.58	0.05	0.00
Methyl linoleate	94	n.d.	4.22	n.d.	6.49	n.d.	0.67	n.d.	1.14	n.d.	n.d.
Thianaphthene	83	0.33	1.00	0.24	0.90	0.26	0.79	0.45	1.81	3.01	1.38

Table 3
Quantitative composition by HPLC-HRMS analysis of **TA1-TA4, VA, RG** and **TA1e-TA4e.** Kruskal-Wallis Test was applied to study differences between groups (**TA**, **VA** and **RG**). Different letters (a, b or c) indicate significant differences between the experimental groups ($p < 0.05$).

Sample	(+)-Catechin	Caffeic acid	Coumaric acid	Ferulic acid	Quercetin-3-O-glucoside	Quercetin-3-O-rutinoside	Abscisic acid	Glutathione
TA1	<0.050	1.827 ± 0.14	0.101 ± 0.01	4.95 ± 0.31	0.073 ± 0.004	0.245 ± 0.011	0.864 ± 0.05	6.84 ± 0.17
TA2	<0.050	2.202 ± 0.15	0.101 ± 0.01	5.47 ± 0.08	0.064 ± 0.004	0.165 ± 0.014	0.959 ± 0.02	2.81 ± 0.05
TA3	<0.050	0.127 ± 0.03	0.096 ± 0.06	3.67 ± 0.18	0.076 ± 0.006	0.223 ± 0.006	1.213 ± 0.07	35.83 ± 0.26
TA4	<0.050	0.150 ± 0.02	0.087 ± 0. 05	4.04 ± 0.14	0.079 ± 0.004	0.25 ± 0.014	0.962 ± 0.07	36.36 ± 0.32
TA mean	<0.050	1.026 ± 0.96[a]	0.078 ± 0.04[a]	4.38 ± 0.82	0.071 ± 0.01[a]	0.215 ± 0.04[a]	0.996 ± 0.14	20.32 ± 16.72 [a]
VA	<0.050	0.254 ± 0.02[b]	1.007 ± 0.22[b]	4.98 ± 0.23	0.088 ± 0.006[a]	0.275 ± 0.015[a]	0.869 ± 0.02	2.37 ± 0.42[b]
RG	<0.050	0.575 ± 0.12[c]	0.979 ± 0.18[b]	4.83 ± 0.34	0.141 ± 0.009[b]	0.462 ± 0.008[b]	1.165 ± 0.09	3.25 ± 0.22[b]
TA1e	<0.050	3.375 ± 0.25	0.771 ± 0.13	5.44 ± 0.11	0.081 ± 0.005	0.282 ± 0.009	1649 ± 0.04	10.59 ± 0.42
TA2e	<0.050	2.782 ± 0.26	0.171 ± 0.02	6.39 ± 0.21	<0.050	0.166 ± 0.008	0.786 ± 0.06	3.30 ± 0.22
TA3e	<0.050	0.385 ± 0.06	0.066 ± 0.02	6.51 ± 0.05	<0.050	0.147 ± 0.005	0.844 ± 0.06	26.18 ± 0.22
TA4e	<0.050	0.236 ± 0.03	0.114 ± 0.03	11.41 ± 0.17	0.054 ± 0.004	0.188 ± 0.014	1227 ± 0.08	36.01 ± 0.36

[a] Data are presented as the mean of three replications and SD are within 10%.

and anti-atherosclerotic activities, was confirmed in **TA** samples, as previously reported (Kim et al., 2017). All these results confirm a distinct phytochemical profile of Tuscan elephant garlic samples, with a different bioactive compound panel and sensorial attributes concerning red garlic.

3.5. Identification and quantitation of dipeptides in TA1e-TA4e via UHPLC-HRMS/MS

To quantify other non-polyphenol, peptidic metabolites, we exploited the UHPLC-ESI-Orbitrap-MS analysis on **TA1e-TA4e** samples. Table S2 shows all metabolites tentatively identified in **TA** extracts: some correspond to those already identified by other techniques (see above) while other bioactives were specifically identified by using this technique. The identification was determined by comparing retention times, and MS data (accurate mass, isotopic distribution, and fragmentation pattern) to the existing literature and by searching the phytochemical dictionary of the natural products database. The metabolites belonged to various classes, including sulphur- and non-sulphur-containing peptides, flavonoids, phenolic acids, and fatty acids, confirming the results of our metabolomic analysis. Their elution order in the chromatogram followed a decreasing polarity, with dipeptides and phenolic acids being eluted first, followed by flavonoid di- and monoglucosides, aglycones, and finally fatty acids. LC-ESI-MS/MS analysis (Table S2) and RP-UHPLC-PDA profiling (Fig. S4) revealed that the **TA** extracts contain a significant amount of γ-glutamyl peptides (Table 4). Specifically, compounds 3, 5, and 7 showed a precursor ion at *m/z* 289 (Fig. S5). The loss of water $[M-H-18]^-$ and subsequent loss of a glutamine residue along the amide linkage, resulted in fragments at *m/z* 271 and *m/z* 128, respectively. Based on these observations, these peaks were tentatively identified as *N*-γ-glutamyl-S-allylcysteine isomers, corresponding to those fragments identified previously in *Allium cepa* and *Allium sativum* (Farag et al., 2017). Furthermore, as in Fig. S6, compounds 4 and 6 exhibiting $[M-H]^-$ ions at *m/z* 259 and fragments at *m/z* 128 were observed, indicating the loss of a glutamine moiety. These peaks correspond to the compound provisionally identified as *N*-γ-glutamylisoleucine.(Farag et al., 2017) Compound 8 (Fig. S7) was tentatively identified as *N*-γ-glutamylphenylalanine, based on the $[M-H]^-$ ions observed at *m/z* 293, as well as the MS/MS fragments observed at *m/z* 128 and *m/z* 275, which correspond to the loss of the glutamine residue and water, respectively (Farag et al., 2017). Additionally, peak 9 was tentatively identified as γ-glutamyl-S-allylthiocysteine (Fig. S8). This identification was supported by the presence of a precursor ion at *m/z* 321, and of a fragment at *m/z* 249, which corresponds to the breakage of the allyl sulphur moiety. Additionally, a fragment at *m/z* 128 was observed, which is attributed to the loss of the glutamine

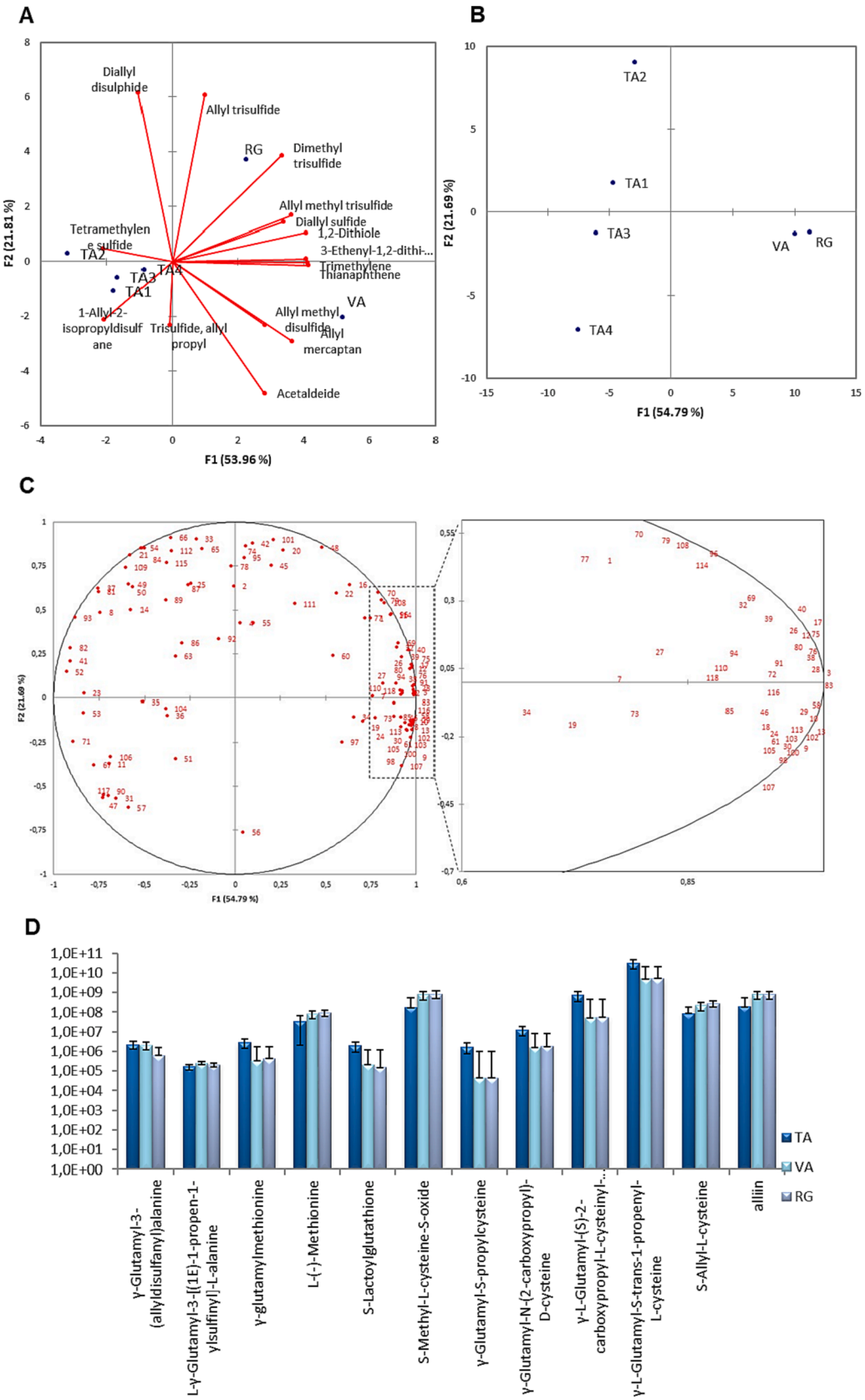

Fig. 1. PCA analysis. A) Biplot of Principal component analysis based on the contents of main sulfur-containing volatile components detected by SPME-GC/MS in **TA**, **VA** and **RG** samples. The biplot describes the different sample origins and the contribution of volatile molecules to the variability among samples; **B,C)** Score plot of PCA analysis (**B**) and loading plots (**C**) with a zoom box to show the contribution of molecules to the sample distribution (variable code numbers correspond to molecules identified and listed in **Table S1**); **D)** Sulfur-containing compounds (expressed as areas normalized to sample weight and on logarithmic scale) in the different samples.

Table 4
Quantitative Profiling of Dipeptides Identified in **TA** Extracts.

Sample	N-γ-Glutamyl-S-allylcysteine	N-γ-Glutamyl-isoleucine	N-γ-Glutamyl-S-allylcysteine	N-γ-Glutamyl-isoleucine	N-γ-Glutamyl-S-allylthiocysteine
TA1e	13.48 ± 0.09^{c}	8.95 ± 0.05^{a}	43.15 ± 0.15^{c}	12.79 ± 0.15^{b}	7.31 ± 0.04^{b}
TA2e	20.07 ± 0.25^{b}	1.22 ± 0.04^{c}	26.02 ± 0.31^{d}	23.40 ± 0.11^{a}	11.73 ± 0.06^{a}
TA3e	20.49 ± 0.11^{a}	1.94 ± 0.05^{b}	73.20 ± 0.51^{b}	12.70 ± 0.07^{b}	7.17 ± 0.08^{b}
TA4e	19.80 ± 0.07^{b}	1.85 ± 0.10^{b}	77.91 ± 0.42^{a}	11.11 ± 0.15^{c}	6.23 ± 0.05^{c}

Data expressed as mean (mg SACE g −1 dried extracts) ± SD (n = 3) SACE: S-Allyl-Cysteine Equivalents. Means followed by different letters are significantly different according to Tukey's honestly significant difference (HSD). Means followed by the same letter are not significantly different.

residue. Furthermore, compound 12 was tentatively identified as 9,12,13-trihydroxyoctadeca-7-enoic acid. This identification was supported by the presence of a $[M-H]^-$ ion at *m/z* 329, as well as a base fragment peak at *m/z* 311, which resulted from the loss of a water molecule. Additional fragment peaks were observed at *m/z* 293, *m/z* 229, and *m/z* 211, which can be attributed to the losses of aliphatic residues. Additionally, a sulphated fatty alcohol was tentatively identified as trimethylnonanol sulphate, corresponding to peak 19. This latter identification was based on the presence of a $[M-H]^-$ ion at *m/z* 265. Saponins are another abundant class of compounds found in TA extracts by UHPLC-HRMS/MS analysis. MS/MS analysis was conducted to identify saponins based on deprotonated sapogenin ions and fragments related to the neutral loss of a glycosyl moiety. Specifically, the neutral loss of 176 or 144 Da corresponds to a hexuronyl or 3-hydroxy-3-methylglutaroyl moiety, respectively. In contrast, the neutral losses of 162, 114 or 132 Da correspond to a hexosyl, glutaroyl or pentosyl moiety, respectively. For instance, compound 14 (**Fig. S4**, **Table S2**) exhibited $[M-H]^-$ ions at *m/z* 817 and MS/MS base fragment ions at *m/z* 771 and *m/z* 609, resulting from the loss of formic acid (46 Da) and a hexosyl (162 Da), respectively. Based on this data, compound 14 was tentatively identified as a sapogenin belonging to subclass IV5 (463 + dh + p + fa) according to the classification system for steroidal sapogenins in genus *Allium*, as previously described using leek as a matrix (Geng et al., 2021).

3.6. ^{1}H NMR analysis

Monodimensional (^{1}H)NMR analysis was conducted on **TA** extracts to confirm the presence of typical bioactives in the samples. In the same experimental conditions, **TA1e-TA4e** showed similar spectra (**Fig. S10**). In particular, these analyses confirmed the presence of different amino acids found in the typical region from 0.90 to 2.48 ppm. Sugars have been identified in all the samples, in the region from 3.50 to 5.26 ppm. These latter showed to be the most abundant components as revealed by the intensity of the diagnostic signals. Other representative compounds were allicin, identified by the multiplet proton at 5.26 ppm (CH-1b) and (+)-catechin (CH_2-4′ found at 2.49 ppm) (**Table S3**).

3.7. Antioxidant profile of TA1e-TA4e: TPC and FRAP assays

The antioxidant profile of **TA1e-TA4e** was assessed using *in vitro* tests. In particular, the TPC assay was performed to evaluate the total phenols, expressed as mg of gallic acid equivalents. All the samples **TA1e-TA4e** showed similar values of TPC in the range of 7.729–8.304 mg of gallic acid equivalents/g sample. The FRAP values showed a similar trend for **TA1e-TA3e**, while **TA4e** displayed a higher ARA percentage compared to the other extracts (**Fig. S9**).

3.8. Nutraceutical profiling: Vasoactivity of TA1e-TA4e in rat aorta rings pretreated with phenylephrine and KCl

In order to proceed to the nutraceutical profiling of elephant garlic, confirming the role of glutathione, several bioassays were performed. The role of red garlic in cardiovascular diseases has been already demonstrated, but no data are available on elephant garlic to date. The following experiments were performed to investigate the effect of **TA** extracts on vascular pharmaco-mechanical coupling. In endothelium-intact preparations, **TA1e-TA4e** caused concentration-dependent vasodilation with E_{max} values of 78.0 ± 22.8 % (n = 6), 62.3 ± 21.4 % (n = 5), 59.1 ± 42.5 % (n = 6), and 60.3 ± 20.2 % (n = 6) (**Fig. S11A**), respectively (Fig. 2A). Endothelium removal weakly affected the efficacy of **TA1e** (55.6 ± 22.8 %, n = 6; P = 0.1196) (Fig. 2B). Similar results were obtained for **TA2e** (45.4 ± 18.6 %, n = 3; P = 0.3023) and **TA3e** (60.9 ± 26.2 %, n = 5; P = 0.9374), while the removal significantly reduced the efficacy of **TA4e** (28.0 ± 3.0 %, n = 3; P = 0.032) (**Fig. S11B**). The addition of KHS did not affect the phenylephrine-induced tone under both experimental conditions. The effects of the nitric oxide synthase inhibitor L-NAME and the soluble guanylyl cyclase inhibitor ODQ were assessed to justify the endothelium-dependent relaxation caused by **TA4e**. Pre-incubation of tissues with either 100 μM L-NAME (Fig. 2C) or 1 μM ODQ (Fig. 2D) caused a significant rightward shift of the concentration–response curve to **TA4e**. DMSO did not modify the vasorelaxant activity of the extract. In preparations stimulated by phenylephrine, the vasodilator effect was, at least in part, linked to the presence of an intact endothelium, especially that of **TA4e**. Endothelial cells produce and release various vasodilating substances, such as nitric oxide (NO), hyperpolarizing factors, and prostaglandins. Once they reach the smooth muscle layer, these evoke vasodilation through various mechanisms: one of the most important is played by the soluble enzyme guanylate cyclase that, once activated by NO, produces cGMP, the cyclic nucleotide responsible for protein kinase G (PKG) activation. This, in turn, phosphorylates several target proteins, including Ca_V channels, ion pumps (e.g., the sarcoplasmic reticulum Ca^{2+}-ATPase), receptors (e.g., IP3), and enzymes (e.g., phospholipase C), all involved in the control of intracellular Ca^{2+} concentration. The experimental evidence here presented is consistent with the activation of the NO synthase/soluble guanylate cyclase pathway, as two specific inhibitors of these actors, namely L-NAME and ODQ, significantly reduced the vasorelaxant activity of **TA4e**. Noticeably, *Allium sativum*-induced vasodilatation, though markedly reduced by soluble guanylate cyclase inhibitors, is not affected by NO synthase inhibition (Ashraf et al., 2004). Therefore, it is conceivable to hypothesize that the high concentration of GSH found in *Allium ampeloprasum* var. *Holmense* **TA4e** (**TA4** GSH ~ 36 mg/Kg vs **RG** GSH = 3.25 mg/Kg, Table 3) is responsible for endothelial nitric oxide synthase stimulation, as reported in the literature (Cheung & Schulz, 1997).

In a subsequent series of experiments, the effects of **TA1e** on Ca^{2+} release from intracellular store sites and Ca^{2+} influx from the extracellular environment triggered by phenylephrine were assessed. Pre-treatment with 1 mg mL^{-1} **TA1e** partially, though not significantly, reduced Ca^{2+} influx triggered by phenylephrine (162.4 ± 24.1 %, n = 5, control, and 125.4 ± 34.5 %, n = 5, **TA1e**; P = 0.4051) without affecting Ca^{2+} release from intracellular store sites (54.9 ± 10.4 %, control, and 47.6 ± 7.4 %, respectively; P = 0.5866). Phenylephrine-induced contraction is due to the release of Ca^{2+} from the IP3-sensitive sarcoplasmic reticulum and to the opening of G protein-activated Ca^{2+} channels and store-operated Ca^{2+} channels: the resulting Ca^{2+} influx causes membrane depolarization and the subsequent opening of $Ca_V1.2$ channels (Fransen et al., 2015). The most effective extract, i.e., **TA1e** did not modify the release of Ca^{2+} from intracellular stores and partially

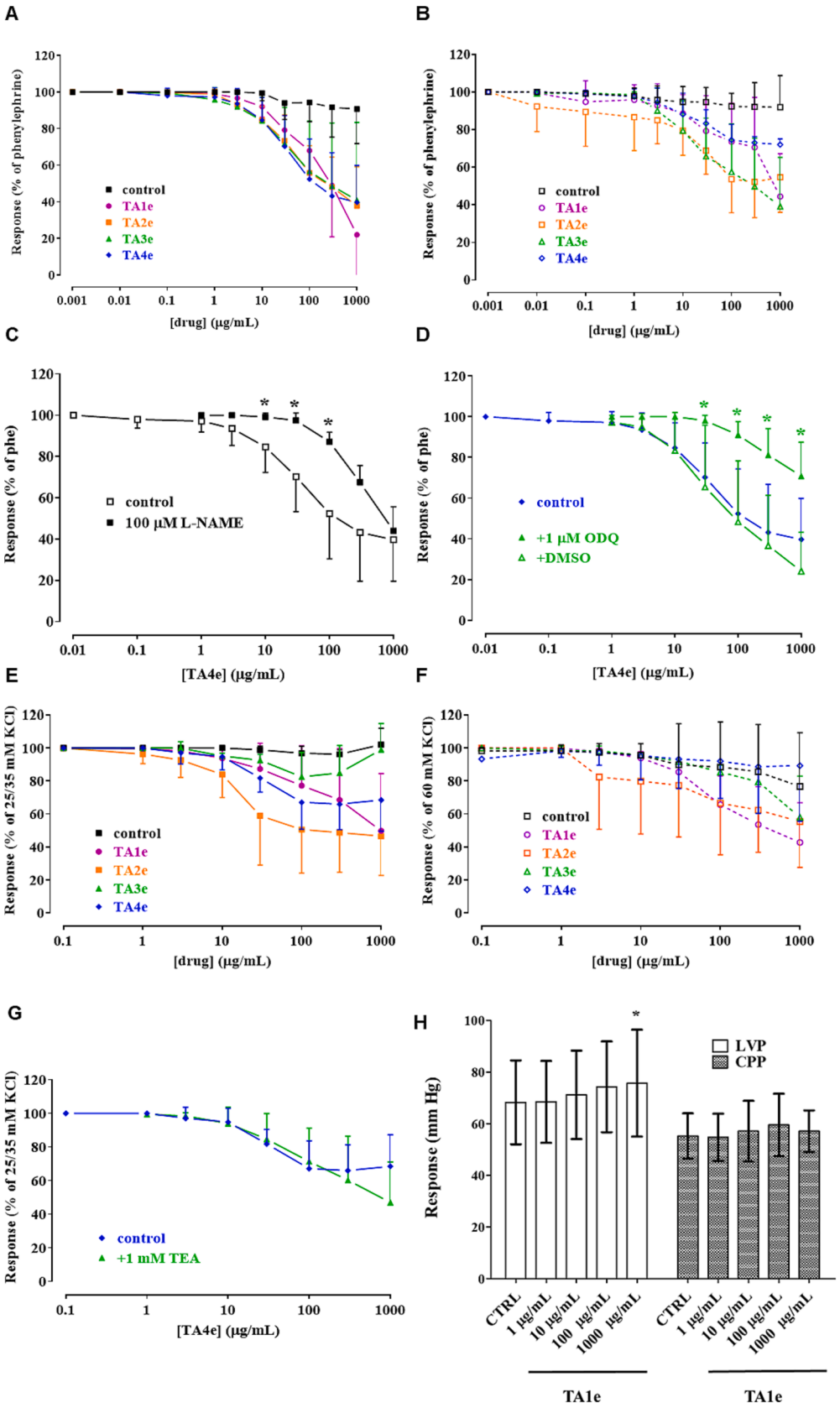

(caption on next page)

Fig. 2. Cardiovascular activity profile of TA1e-TA4e. A,B) TA1e-TA4e relaxed phenylephrine-induced contraction of rat aorta rings; Concentration-response curves of **TA1e-TA4e** on (**A**) endothelium-intact or (**B**) endothelium-denuded preparations. The effect of vehicle (control) is also shown. In the ordinate scale, relaxation is reported as a percentage of the initial tension induced by phenylephrine. Data are mean ± S.D. (n = 3–6). **C,D) L-NAME and ODQ antagonized TA4e-induced endothelium-dependent relaxation of rat aorta rings;** Concentration-response curves to **TA4e** on endothelium-intact preparations pre-contracted by 0.3 μM phenylephrine, either in the absence (control) or in the presence of (**C**) 100 μM L-NAME or (**D**) 1 μM ODQ, pre-incubated for 20 min. In the ordinate scale, relaxation is reported as a percentage of the initial tension induced by phenylephrine. Data points are means ± S.D. (n = 4–5). **E-G) TA1e-TA4e relaxed KCl-induced contraction of rat aorta rings.** (**E,F**) Concentration-response curves to **TA1e-TA4e** in endothelium-denuded preparations pre-contracted by either (**E**) 25/35 mM or (**F**) 60 mM KCl. The effect of vehicle (control) is also shown. (**G**) TEA did not modify the vasorelaxant effect of **TA4e**. Concentration-response curves to **TA4e** in endothelium-denuded preparations, pre-contracted by 25/35 mM KCl, constructed in the absence (control) or presence of 1 mM TEA. The control curve is the same as shown in panel A. In the ordinate scale, relaxation is reported as a percentage of the initial tension induced by KCl. Data are mean ± S.D. (n = 3–7). **H) Effects TA1e on LVP and CPP in Langendorff-perfused rat hearts.** Concentration-effect relationship of **TA1e** on LVP and CPP. On the ordinate scale, the response is reported as mmHg. Each value represents mean ± SD (n = 7). *P < 0.05, repeated measures ANOVA and Dunnet post-hoc test.

reduced the influx of extracellular Ca^{2+} induced by phenylephrine, suggesting that the vascular activity of **TA1e** occurred mostly at the plasma membrane level. Furthermore, as the antispasmodic effect was lower as compared to the spasmolytic one, it is possible that during the pre-incubation period, some volatile vasorelaxant agents were lost.

The vasorelaxant activity of **TA1e-TA4e** was also assessed on rings pre-contracted by either moderate (25–35 mM) or high (60 mM) KCl concentrations, which cause membrane depolarization and $Ca_V1.2$ channel opening. Under both experimental conditions, the most effective extract was **TA1e**, showing E_{max} values of 50.2 ± 34.6 % (n = 7) and 57.3 ± 24.0 % (n = 5), respectively (Fig. 2E-F). In rings stimulated by 25–35 mM KCl, only **TA2e** showed a vasorelaxant activity comparable to that of **TA1e** (E_{max} value of 53.5 ± 23.8 %, n = 5). As **TA4e** was more effective on the contraction induced by moderate than high concentrations of KCl, its vasorelaxant activity was assessed in the presence of the K^+ channel blocker TEA. However, the concentration-relaxation curve constructed in the presence of TEA overlapped that obtained in its absence (Fig. 2G).

The spasmolytic effect observed in preparations stimulated with either high or moderate concentrations of KCl suggested that **TA1e** and **TA3e** might contain some molecules endowed with Ca^{2+} antagonistic activity whereas **TA2e** and **TA4e** might include some K^+ channel openers. In fact, their vasorelaxant activity was directly and indirectly correlated, respectively, to the transmembrane K^+ gradient, a behaviour previously revealed by Gurney *(*Gurney, 1994*)*. Garlic, as well as the four *Allium ampeloprasum* var. *Holmense* samples here examined, are known to contain several compounds capable of releasing the gasotransmitter H_2S that, as demonstrated by Zhao *et al. (*Zhao et al., 2001*)*, in vascular smooth muscle cells stimulates ATP-dependent K^+ channels causing membrane hyperpolarization and vasodilation. The gasotransmitter can also modify the activity of other K^+ channels, such as K_V7, intracellular pH, the activity of phosphodiesterases and, consequently, that of cGMP. Nevertheless, $K_{Ca}1.1$ channels seem not involved in this phenomenon, as the blocker TEA did not affect **TA4e** vasorelaxation. All this evidence could be linked to the additive or synergic effect of several molecules present in the elephant garlic extracts, however, pointing out the nutraceutical value of elephant garlic (**TA**).

3.9. Effects of TA1e on Langendorff perfused rat heart

For Langendorff perfused rat heart experiments, studying the cardiac function and ECG, **TA1e** was selected. Selection criteria were based on the efficacy of **TA1e** in phenylephrine-induced contraction. Under control conditions, LVP and CPP values of 68.3 ± 16.2 and 55.3 ± 8.7 mmHg (n = 7), respectively, were obtained (Fig. 2H). At the maximum concentration tested (1000 μg/mL), **TA1e** significantly increased LVP, decreased HR and prolonged RR interval (**Table S4**). However, CPP, and PQ, QRS and QTc interval values did not vary over the extract concentration range tested (Fig. 2H, **Table S4**). Therefore, **TA1e** exhibited positive inotropic and negative chronotropic properties that may be useful in ischemia–reperfusion injury and in congestive heart failure.

4. Conclusion

To the best of our knowledge, this is the first multi-analytical investigation for geographical authentication of Tuscany elephant garlic (**TA**) *Allium ampeloprasum* L., Italian food excellence, by combining SIR, HPLC-HRMS, SPME-GC/MS, NMR, chemometric and biological functional studies. The stable isotopic ratios (in particular δ^2H and $\delta^{18}O$ values) allow a good geographical characterization of **TA** compared to common garlic samples from different parts of the world. Furthermore, **TA** samples shared a similar chemical composition, with aminoacids, (+)-catechin, cinnamic acids, and quercetin glycosides as major components. Interestingly, the different distribution of sulfur-containing molecules and the higher sugar levels of **TA** samples as compared to those of the other Allium types, highlighted the unicity of **TA** food product. GSH, present in a significant percentage, is proposed as a molecular marker for elephant garlic. The nutraceutical profiling of **TA** demonstrated that **TA4e**, containing a high amount of GSH, possessed a noticeable spasmolytic activity mediated by the release of NO from the endothelium, while **TA1e** an interesting positive inotropic and negative chronotropic effect. These properties, combined with the antioxidant activity of metabolites, highlight the nutraceutical potential of this food excellence cultivated in Tuscany that might prevent the onset of cardiovascular diseases. Further investigations, including a much higher number of samples over 2–3 years of production, will be conducted to study the intra-annual variability and to test other statistical models to better discriminate the geographical origin of samples.

CRediT authorship contribution statement

Gabriele Carullo: Writing – review & editing, Writing – original draft, Supervision, Methodology, Investigation, Formal analysis, Data curation, Conceptualization. **Francesca Borghini:** Formal analysis, Data curation. **Fabio Fusi:** Methodology, Investigation. **Simona Saponara:** Methodology, Investigation. **Anna Fontana:** Investigation. **Luca Pozzetti:** Methodology, Investigation. **Riccardo Fedeli:** Data curation. **Alice Panti:** Formal analysis. **Beatrice Gorelli:** Investigation, Data curation. **Giovanna Aquino:** Software, Methodology. **Manuela Giovanna Basilicata:** Investigation, Methodology, Software. **Giacomo Pepe:** Writing – original draft, Methodology, Formal analysis. **Pietro Campiglia:** Formal analysis. **Stefano Biagiotti:** Methodology, Formal analysis. **Sandra Gemma:** Writing – review & editing, Resources, Investigation. **Stefania Butini:** Methodology, Formal analysis. **Silvia Pianezze:** Methodology, Investigation. **Stefano Loppi:** Methodology, Formal analysis. **Alessandro Cavaglioni:** Investigation, Formal analysis, Data curation. **Matteo Perini:** Writing – review & editing, Writing – original draft, Methodology, Investigation, Formal analysis. **Giuseppe Campiani:** Writing – review & editing, Writing – original draft, Funding acquisition, Formal analysis, Data curation, Conceptualization.

Declaration of competing interest

The authors declare that they have no known competing financial interests or personal relationships that could have appeared to influence

the work reported in this paper.

Data availability

Data will be made available on request.

Appendix A. Supplementary material

Supplementary data to this article can be found online at https://doi.org/10.1016/j.foodchem.2024.138684.

References

Ahmed, A., Trezza, A., Gentile, M., Paccagnini, E., Panti, A., Lupetti, P., Spiga, O., Bova, S., & Fusi, F. (2023). Dynamin-independent CaV1.2 and KCa1.1 channels regulation and vascular tone modulation by the mitochondrial fission inhibitors dynasore and dyngo-4a. *European Journal of Pharmacology, 951*, Article 175786. https://doi.org/10.1016/J.EJPHAR.2023.175786

Araguas Araguas, L., Danesi, P., Froehlich, K., & Rozanski, K. (1996). Global monitoring of the isotopic composition of precipitation. *Journal of Radioanalytical and Nuclear Chemistry, 205*(2), 189–200. https://doi.org/10.1007/BF02039404/METRICS

Ashraf, M. Z., Hussain, M. E., & Fahim, M. (2004). Endothelium mediated vasorelaxant response of garlic in isolated rat aorta: Role of nitric oxide. *Journal of Ethnopharmacology, 90*(1), 5–9. https://doi.org/10.1016/j.jep.2003.06.001

Bateman, A. S., Kelly, S. D., & Woolfe, M. (2007). Nitrogen isotope composition of organically and conventionally grown crops. *Journal of Agricultural and Food Chemistry, 55*, 2664–2670. https://doi.org/10.1021/jf0627726

Barbour, M. M. (2007). Stable oxygen isotope composition of plant tissue: A review. *Functional Plant Biology: FPB, 34*(2), 83–94. https://doi.org/10.1071/FP06228

Bosona, T., & Gebresenbet, G. (2013). Food traceability as an integral part of logistics management in food and agricultural supply chain. *Food Control, 33*(1), 32–48. https://doi.org/10.1016/J.FOODCONT.2013.02.004

Bowen, G. J., Ehleringer, J. R., Chesson, L. A., Stange, E., & Cerling, T. E. (2007). Stable isotope ratios of tap water in the contiguous United States. *Water Resources Research, 43*(3). https://doi.org/10.1029/2006WR005186

Çakmakçı, S., & Çakmakçı, R. (2023). Quality and Nutritional Parameters of Food in Agri-Food Production Systems. *Foods 2023, Vol. 12, Page 351*, *12*(2), 351. https://doi.org/10.3390/FOODS12020351.

Carullo, G., Ahmed, A., Trezza, A., Spiga, O., Brizzi, A., Saponara, S., Fusi, F., & Aiello, F. (2021). A multitarget semi-synthetic derivative of the flavonoid morin with improved in vitro vasorelaxant activity: Role of $Ca_V1.2$ and $K_{Ca}1.1$ channels. *Biochemical Pharmacology, 185*, Article 114429. https://doi.org/10.1016/j.bcp.2021.114429

Ceccanti, C., Rocchetti, G., Lucini, L., Giuberti, G., Landi, M., Biagiotti, S., & Guidi, L. (2021). Comparative phytochemical profile of the elephant garlic (Allium ampeloprasum var. holmense) and the common garlic (Allium sativum) from the Val di Chiana area (Tuscany, Italy) before and after in vitro gastrointestinal digestion. *Food Chemistry, 338*. https://doi.org/10.1016/J.FOODCHEM.2020.128011

Cheung, P. Y., & Schulz, R. (1997). Glutathione causes coronary vasodilation via a nitric oxide- and soluble guanylate cyclase-dependent mechanism. *The American Journal of Physiology, 273*(3 Pt 2), H1231–H1238. https://doi.org/10.1152/ajpheart.1997.273.3.H123

Danezis, G. P., Tsagkaris, A. S., Camin, F., Brusic, V., & Georgiou, C. A. (2016). Food authentication: Techniques, trends & emerging approaches. *TrAC Trends in Analytical Chemistry, 85*, 123–132. https://doi.org/10.1016/J.TRAC.2016.02.026

Fanelli, V., Mascio, I., Miazzi, M. M., Savoia, M. A., De Giovanni, C., & Montemurro, C. (2021). Molecular Approaches to Agri-Food Traceability and Authentication: An Updated Review. *Foods 2021, Vol. 10, Page 1644*, *10*(7), 1644. https://doi.org/10.3390/FOODS10071644.

Farag, M. A., Ali, S. E., Hodaya, R. H., El-Seedi, H. R., Sultani, H. N., Laub, A., Eissa, T. F., Abou-Zaid, F. O. F., & Wessjohann, L. A. (2017). Phytochemical Profiles and Antimicrobial Activities of Allium cepa Red cv. and A. sativum Subjected to Different Drying Methods: A Comparative MS-Based Metabolomics. *Molecules 2017, Vol. 22, Page 761*, *22*(5), 761. https://doi.org/10.3390/MOLECULES22050761.

Fedeli, R., Celletti, S., Loppi, S., & Vannini, A. (2023). Comparison of the Effect of Solid and Liquid Digestate on the Growth of Lettuce (Lactuca sativa L.) Plants. *Agronomy, 13*(3), 782. https://doi.org/10.3390/AGRONOMY13030782/S1

Fedeli, R., Vannini, A., Grattacaso, M., & Loppi, S. (2023). Wood distillate (pyroligneous acid) boosts nutritional traits of potato tubers. *Annals of Applied Biology*. https://doi.org/10.1111/AAB.12837

Fransen, P., Van Hove, C. E., Leloup, A. J. A., Martinet, W., De Meyer, G. R. Y., Lemmens, K., Bult, H., & Schrijvers, D. M. (2015). Dissecting out the complex Ca2+-mediated phenylephrine-induced contractions of mouse aortic segments. *PLoS One1, 10*(3), 1–17. https://doi.org/10.1371/journal.pone.0121634

Fusi, F., Durante, M., Sgaragli, G., Khanh, P. N., Son, N. T., Huong, T. T., Huong, V. N., & Cuong, N. M. (2015). In vitro vasoactivity of zerumbone from Zingiber zerumbet. *Planta Medica, 81*(4), 298–304. https://doi.org/10.1055/S-0034-1396307/BIB

Fusi, F., Durante, M., Gorelli, B., Perrone, M. G., Colabufo, N. A., & Saponara, S. (2017). MC225, a Novel Probe for P-glycoprotein PET Imaging at the Blood-brain Barrier. In Vitro Cardiovascular Safety Evaluation. *Journal of Cardiovascular Pharmacology, 70*(6), 405–410. https://doi.org/10.1097/FJC.0000000000000536

Fusi, F., Ferrara, A., Zalatnai, A., Molnar, J., Sgaragli, G., & Saponara, S. (2008). Vascular activity of two silicon compounds, ALIS 409 and ALIS 421, novel multidrug-resistance reverting agents in cancer cells. *Cancer Chemotherapy and Pharmacology, 61*(3), 443–451. https://doi.org/10.1007/S00280-007-0488-6/FIGURES/5

García-Villalón, A. L., Amor, S., Monge, L., Fernández, N., Prodanov, M., Muñoz, M., … Granado, M. (2016). In vitro studies of an aged black garlic extract enriched in S-allylcysteine and polyphenols with cardioprotective effects. *Journal of Functional Foods, 27*, 189–200. https://doi.org/10.1016/j.jff.2016.08.062

Geng, P., Chen, P., Lin, L. Z., Sun, J., Harrington, P., & Harnly, J. M. (2021). Classification of structural characteristics facilitate identifying steroidal saponins in Alliums using ultra-high performance liquid chromatography high-resolution mass spectrometry. *Journal of Food Composition and Analysis, 102*, Article 103994. https://doi.org/10.1016/J.JFCA.2021.103994

Gurney, A. M. (1994). Mechanisms of Drug-induced Vasodilation. *Journal of Pharmacy and Pharmacology, 46*, 242–251.

Gussow, K. E., & Mariët, A. (2022). The scope of food fraud revisited. *Crime, Law and Social Change, 78*(5), 621–642. https://doi.org/10.1007/S10611-022-10055-W/TABLES/3

Kim, S., Kim, D. B., Jin, W., Park, J., Yoon, W., Lee, Y., Kim, S., Lee, S., Kim, S., Lee, O. H., Shin, D., & Yoo, M. (2017). Comparative studies of bioactive organosulphur compounds and antioxidant activities in garlic (Allium sativum L.), elephant garlic (Allium ampeloprasum L.) and onion (Allium cepa L.). *Https://Doi.Org/10.1080/14786419.2017.1323211*, *32*(10), 1193–1197. https://doi.org/10.1080/14786419.2017.1323211.

Li, J., Dadmohammadi, Y., & Abbaspourrad, A. (2022). Flavor components, precursors, formation mechanisms, production and characterization methods: Garlic, onion, and chili pepper flavors. *Critical Reviews in Food Science and Nutrition, 62*(30), 8265–8287. https://doi.org/10.1080/10408398.2021.1926906

Liu, H., Nie, J., Liu, Y., Wadood, S. A., Rogers, K. M., Yuan, Y., & Gan, R. Y. (2023). A review of recent compound-specific isotope analysis studies applied to food authentication. *Food Chemistry, 415*. https://doi.org/10.1016/J.FOODCHEM.2023.135791

Liu, T. S., Lin, J. N., & Peng, T. R. (2018). Discrimination of Geographical Origin of Asian Garlic Using Isotopic and Chemical Datasets under Stepwise Principal Component Analysis. *Journal of Forensic Sciences, 63*(5), 1366–1373. https://doi.org/10.1111/1556-4029.13731

Loppi, S., Fedeli, R., Canali, G., Guarnieri, M., Biagiotti, S., & Vannini, A. (2021a). Comparison of the Mineral and Nutraceutical Profiles of Elephant Garlic (Allium ampeloprasum L.) Grown in Organic and Conventional Fields of Valdichiana, a Traditional Cultivation Area of Tuscany, Italy. *Biology 2021, Vol. 10, Page 1058*, *10*(10), 1058. https://doi.org/10.3390/BIOLOGY10101058.

Molyneux, R. J. (2017). Traceability of Food Samples: Provenance, Authentication, and Curation. *Journal of Agricultural and Food Chemistry, 65*(41), 8977–8978. https://doi.org/10.1021/ACS.JAFC.7B04214/ASSET/IMAGES/ACS.JAFC.7B04214.SOCIAL.JPEG_V03

Nie, J., Shao, S., Zhang, Y., Li, C., Liu, Z., Rogers, K. M., Wu, M. C., Lee, C. P., & Yuan, Y. (2021). Discriminating protected geographical indication Chinese Jinxiang garlic from other origins using stable isotopes and chemometrics. *Journal of Food Composition and Analysis, 99*, Article 103856. https://doi.org/10.1016/J.JFCA.2021.103856

Olsen, P., & Borit, M. (2013). How to define traceability. *Trends in Food Science & Technology, 29*(2), 142–150. https://doi.org/10.1016/J.TIFS.2012.10.003

Opatić, A. M., Nečemer, M., Kocman, D., & Lojen, S. (2017). Geographical Origin Characterization of Slovenian Organic Garlic Using Stable Isotope and Elemental Composition Analyses. *Acta Chimica Slovenica, 64*(4), 1048–1055. https://doi.org/10.17344/ACSI.2017.3476

Pasqualone, A., Di Rienzo, V., Nasti, R., Blanco, A., Gomes, T., & Montemurro, C. (2013). Traceability of Italian Protected Designation of Origin (PDO) table olives by means of microsatellite molecular markers. *Journal of Agricultural and Food Chemistry, 61*(12), 3068–3073. https://doi.org/10.1021/JF400014G/ASSET/IMAGES/MEDIUM/JF-2013-00014G_0003.GIF

Pessina, F., Gamberucci, A., Chen, J., Liu, B., Vangheluwe, P., Gorelli, B., Lorenzini, S., Spiga, O., Trezza, A., Sgaragli, G., & Saponara, S. (2018). Negative chronotropism, positive inotropism and lusitropism of 3,5-di-t-butyl-4-hydroxyanisole (DTBHA) on rat heart preparations occur through reduction of RyR2 Ca(2+) leak. *Biochemical Pharmacology, 155*, 434–443. https://doi.org/10.1016/j.bcp.2018.07.026

Pianezze, S., Perini, M., Bontempo, L., Ziller, L., & D'Archivio, A. A. (2019). Geographical discrimination of garlic (Allium Sativum L.) based on Stable isotope ratio analysis coupled with statistical methods: The Italian case study. *Food and Chemical Toxicology, 134*, Article 110862. https://doi.org/10.1016/J.FCT.2019.110862

Pozzetti, L., Ferrara, F., Marotta, L., Gemma, S., Butini, S., Benedusi, M., Fusi, F., Ahmed, A., Pomponi, S., Ferrari, S., Perini, M., Ramunno, A., Pepe, G., Campiglia, P., Valacchi, G., Carullo, G., & Campiani, G. (2022). Extra Virgin Olive Oil Extracts of Indigenous Southern Tuscany Cultivar Act as Anti-Inflammatory and Vasorelaxant Nutraceuticals. *Antioxidants, 11*(3), 437. https://doi.org/10.3390/ANTIOX11030437/S1

Rubenstein, D. R., & Hobson, K. A. (2004). From birds to butterflies: Animal movement patterns and stable isotopes. *Trends in Ecology & Evolution, 19*(5), 256–263. https://doi.org/10.1016/J.TREE.2004.03.017

Saponara, S., Ferrara, A., Gorelli, B., Shah, A., Kawase, M., Motohashi, N., Molnar, J., Sgaragli, G., & Fusi, F. (2007). 3,5-dibenzoyl-4-(3-phenoxyphenyl)-1,4-dihydro-2,6-dimethylpyridine (DP7): A new multidrug resistance inhibitor devoid of effects on

Langendorff-perfused rat heart. *European Journal of Pharmacology, 563*(1–3), 160–163. https://doi.org/10.1016/j.ejphar.2007.02.001

Takashima, M., Kanamori, Y., Kodera, Y., Morihara, N., & Tamura, K. (2017). Aged garlic extract exerts endothelium-dependent vasorelaxant effect on rat aorta by increasing nitric oxide production. *Phytomedicine, 24*, 56–61. https://doi.org/10.1016/J.PHYMED.2016.11.016

Zhao, W., Zhang, J., Lu, Y., & Wang, R. (2001). The vasorelaxant effect of H2S as a novel endogenous gaseous KATP channel opener. *The EMBO Journal, 20*(21), 6008–6016. https://doi.org/10.1093/EMBOJ/20.21.6008